TA ČR project TK05020137 “Development of the play-fairway system for the low-temperature geothermal system exploration in sedimentary basins; with application to the Vienna Basin“

End-of-the-year-2024 progress report

Planned Aim

Aim of the project is to develop the play-fairway-map construction technique for low-temperature geothermal systems in sedimentary basins in the GIS environment. The goal is to parameterize the exploration by the system of factors characterizing the geothermal system, its efficiency and its engineering geology characteristics, such as production index for specific power producing technology, reinjection index, environmental impact index and cost index for specific technology; to subsequently normalize those factors and, finally, combine them in such a way that the color-coded play fairway map indicates areas of the basin with the best potential for the geothermal system commercialization, fair potential, poor potential and areas lacking data allowing their evaluation.

Planned Schedule

The project schedule is set for 2 years. Stage 1 of the project (March 2023 – March 2024) is focused on the development of the database, which contains structural geology, lithological, thermal and geochemical data. The development includes a map visualization of the aforementioned data. The data are planned to be collected from about 400 hydrocarbon exploration/production wells located in the Czech portion of the Vienna Basin. Stages 2-3 of the project (March 2024 – March 2025) include: Stage 2 focused on the parameterization of the factors controlling the existence of low-temperature geothermal systems in the study area and risks associated with their successful commercialization and Stage 3 focused on the development of the Arc GIS-based play fairway map.

Results developed by the end of the year 2023

The research team composed of the Technical University Ostrava (TUO) group and Moravské Naftové Doly (MND) group spent the time interval of January – December 2024 on:
1) the interpretation of four stratigraphies that include all main producing reservoirs (lower Badenian, middle Badenian, upper Badenian and Sarmatian stratigraphies) in ten profiles through the reflection seismic volume (**Figs. 1-10**);
2) the second cycle of the Arc GIS visualization of the well-based thermal data (**Figs. 11-12**);
3) the Arc GIS visualization of the density of geothermal fluids analyzed from well samples and associated values of total dissolved solids (**Figs. 13-21**);

4) the interpretation of types and geometries of encountered geothermal fluid flow systems (**Figs. 13-21**); and
5) the calculation of parameters, which will be used for the play fairway map development during January-March 2025 (**Fig. 23**).

All four aforementioned top surfaces of lower Badenian, middle Badenian, upper Badenian and Sarmatian strata were interpreted from the reflection seismic imagery, using programs Kingdom Suite and Petrel, together with faults that deform them. Interpreted profiles also contain projected wells located in their close vicinity. The horizon interpretation in profiles is constrained by depths of horizon penetration in the aforementioned wells.

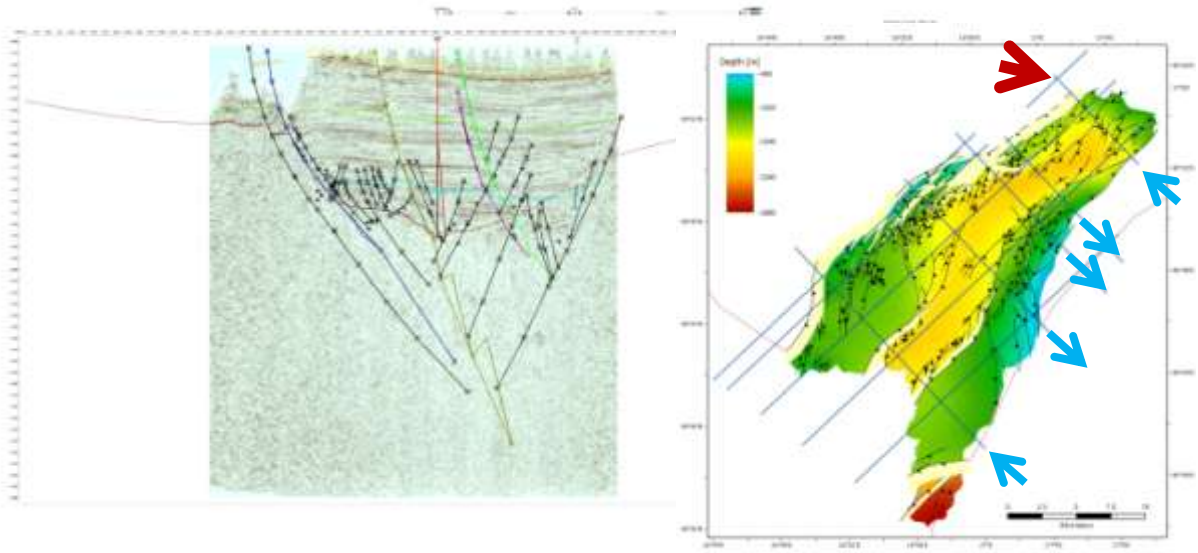

Fig. 1. Interpreted NW-SE oriented reflection seismic profile IL 260. Layer stratigraphy (represented by top surfaces): light yellow – Pontian, dark yellow – Pannonian, green – Sarmatian, light blue – upper Badenian, medium dark blue – middle Badenian, dark blue – lower Badenian, orange – Karpatian, violet – Ottnangian, purple – Eggenburgian. Red arrow shows the profile location. Blue arrow shows the direction of assumed geothermal fluid flow, using the premise that it is controlled by the thermolift up in layers.

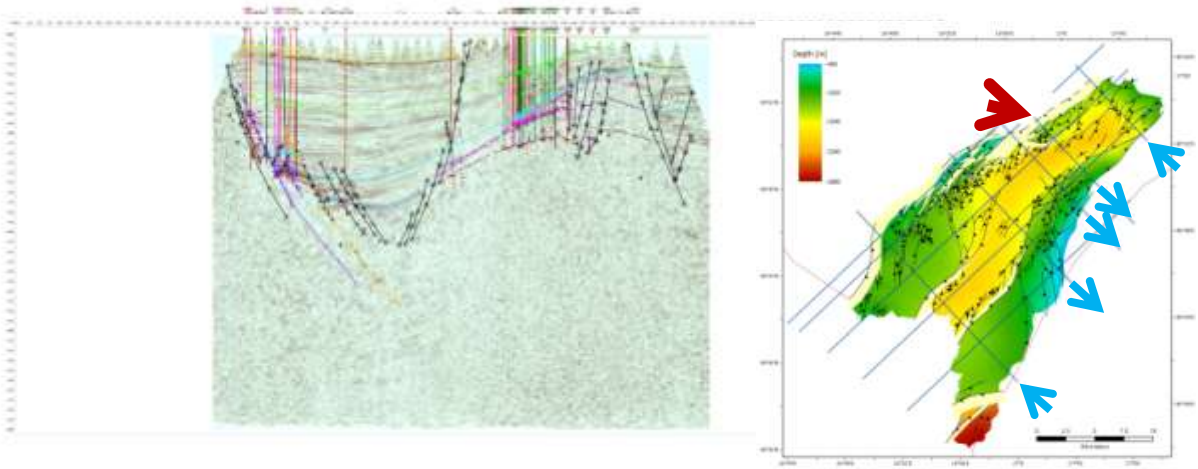

Fig. 2. Interpreted NW-SE oriented reflection seismic profile IL 545. See Fig. 1 for further explanation.

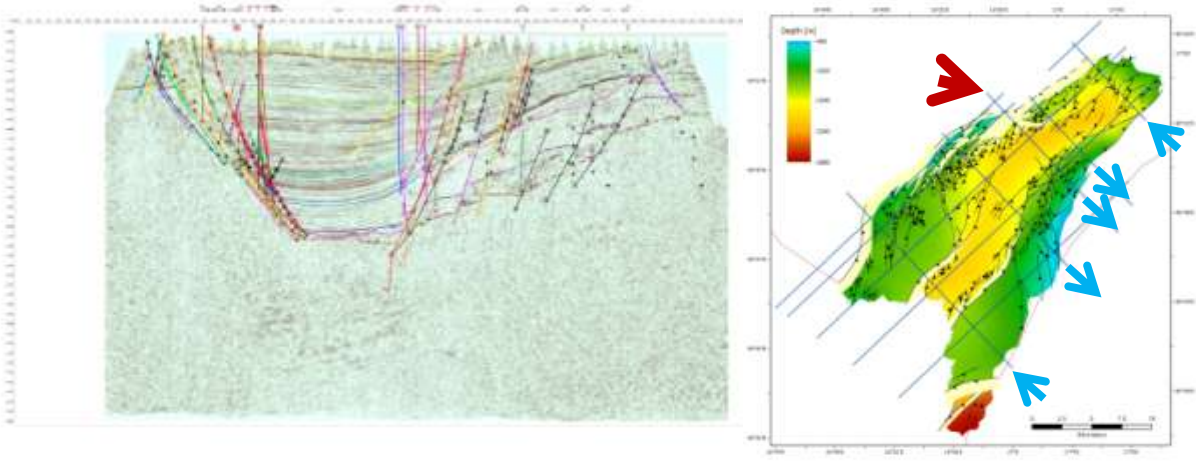

Fig. 3. Interpreted NW-SE oriented reflection seismic profile IL 665. See Fig. 1 for further explanation.

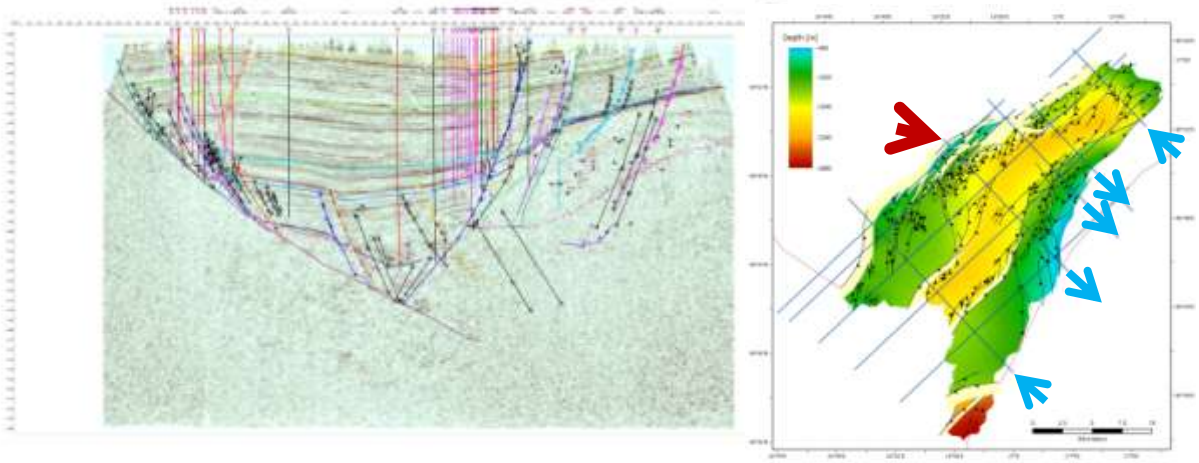

Fig. 4. Interpreted NW-SE oriented reflection seismic profile IL 915. See Fig. 1 for further explanation.

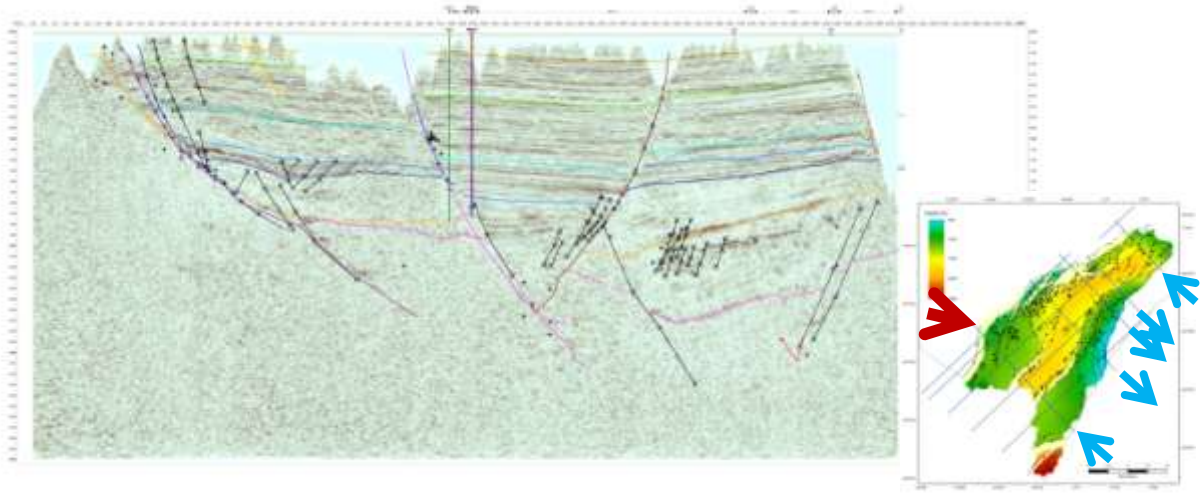

Fig. 5. Interpreted NW-SE oriented reflection seismic profile IL 1375. See Fig. 1 for further explanation.

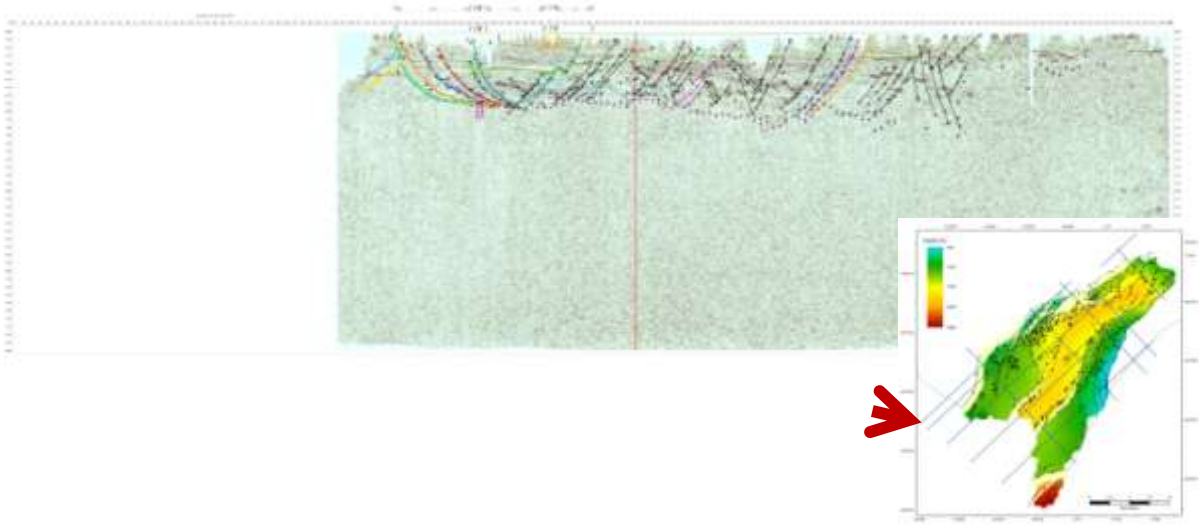

Fig. 6. Interpreted NE-SW oriented reflection seismic profile XL 535. See Fig. 1 for further explanation.

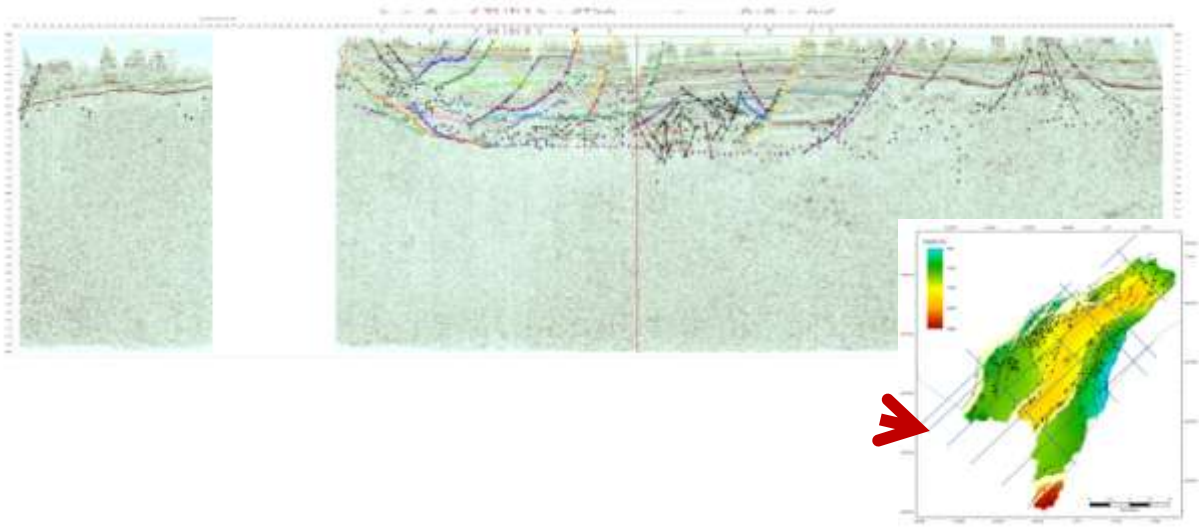

Fig. 7. Interpreted NE-SW oriented reflection seismic profile XL 595. See Fig. 1 for further explanation.

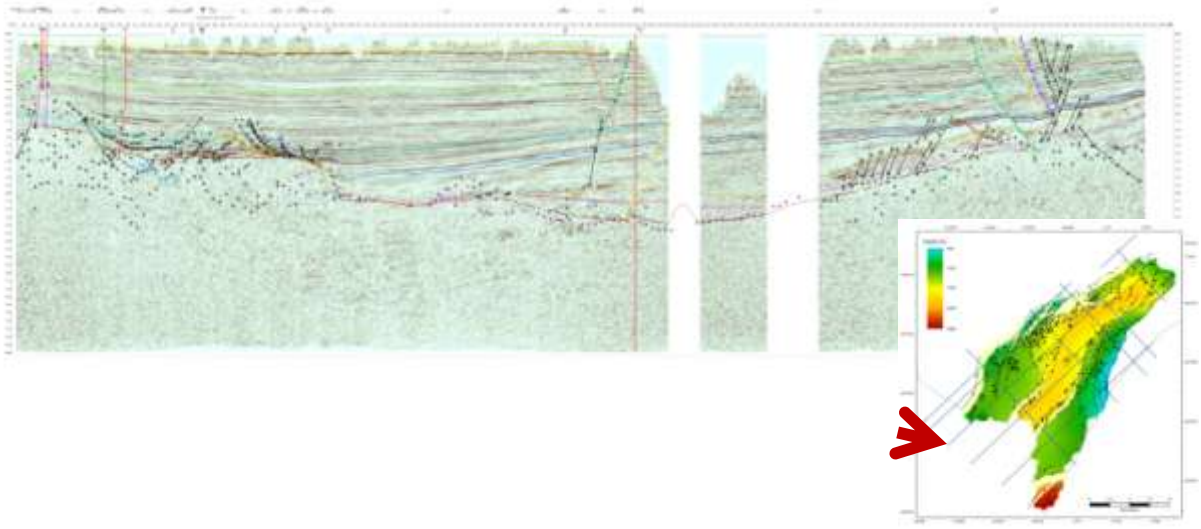

Fig. 8. Interpreted NE-SW oriented reflection seismic profile XL 745. See Fig. 1 for further explanation.

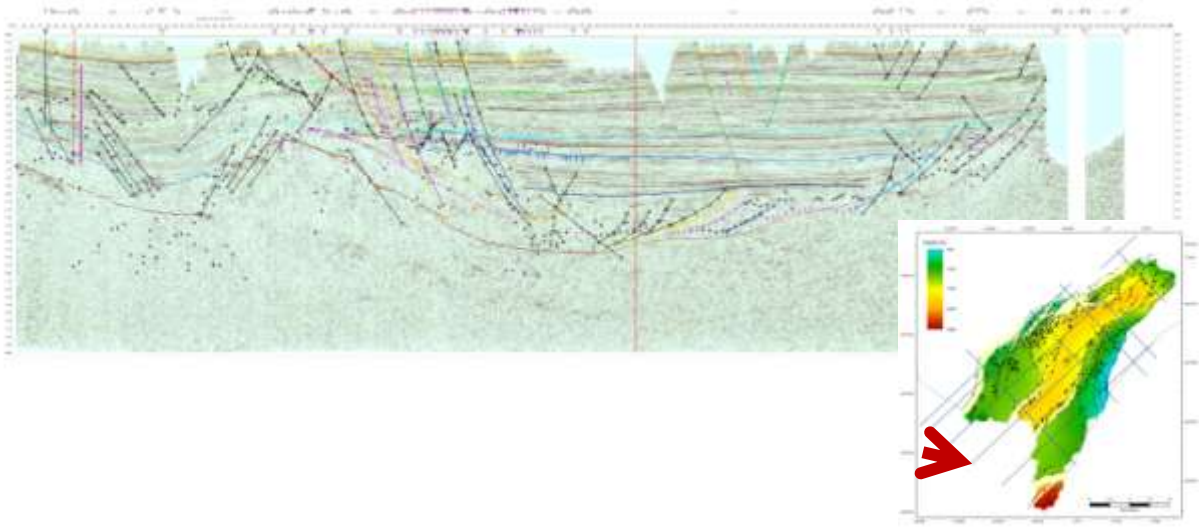

Fig. 9. Interpreted NE-SW oriented reflection seismic profile XL 930. See Fig. 1 for further explanation.

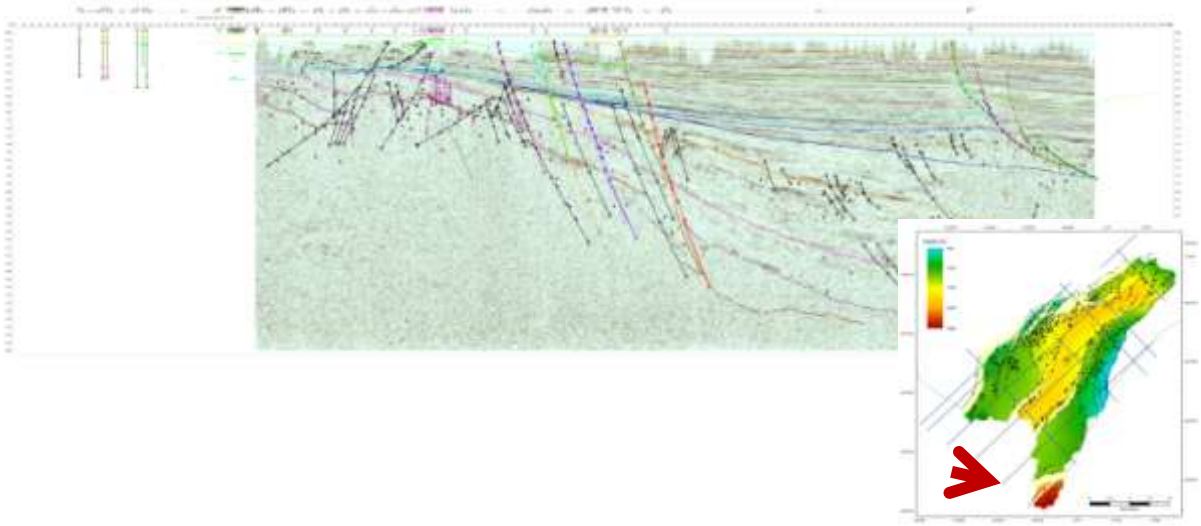

Fig. 10. Interpreted NE-SW oriented reflection seismic profile XL 1160. See Fig. 1 for further explanation.

Figs. 11-12 show two map examples from the final cycle of the visualization of temperature data into maps of temperature distribution at several depths. These two are made for depths of 500 and 1, 000m. The contouring in **Fig. 11** made for a depth of 500 m is developed from thirteen data points. The figure clearly indicates a significant warming in the area of the Hodonín-Gbely horst in the east, located in the center of the Vienna Basin. It also indicates cooling along the NW flank of the basin. While the temperature values characterizing the background basin conditions range from 29 to 31^{o} C, the aforementioned anomalies are characterized by temperature ranges of 25-27 and 32-35^{o} C. We interpret warming as caused by the geothermal fluid discharge, and cooling as caused by the meteoric water recharge. Both areas represent parts of the gravity (topography)-driven geothermal fluid flow system. Arrow in Fig. 11 shows the interpreted vector of the fluid flow from recharge area to discharge area.

Fig. 12 shows even more pronounced temperature difference between recharge and discharge areas, reaching up to 16^{o} C. This difference is in accordance with general knowledge about gradients between recharge and discharge areas increasing with depth.

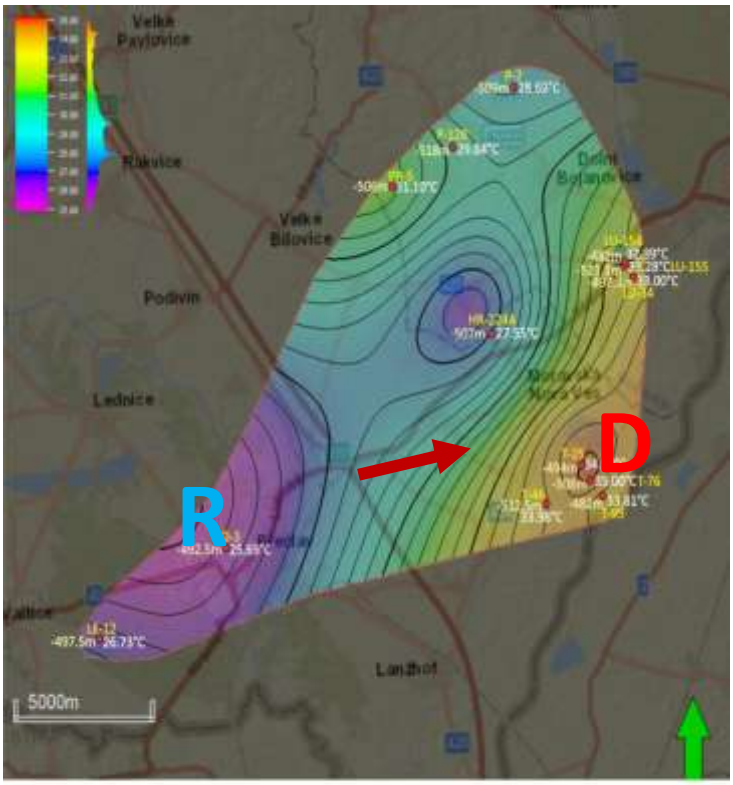

Temperature Contour Map at VB 520, 480m Depth:

White numbers indicate temperatures in degrees Celsius at the specified depth.
Yellow text denotes the well name.
Light yellow numbers represent the structural depth in meters.

Fig. 11. Temperature distribution at a depth of 500 m in the study area. Red dots with numbers represent the input data grid used for contouring. Temperature datum and a depth of its occurrence are shown in white a light yellow. Well name is shown in dark yellow. D and R denote discharge and recharge areas. Red arrow shows the vector of the flow between the two aforementioned areas.

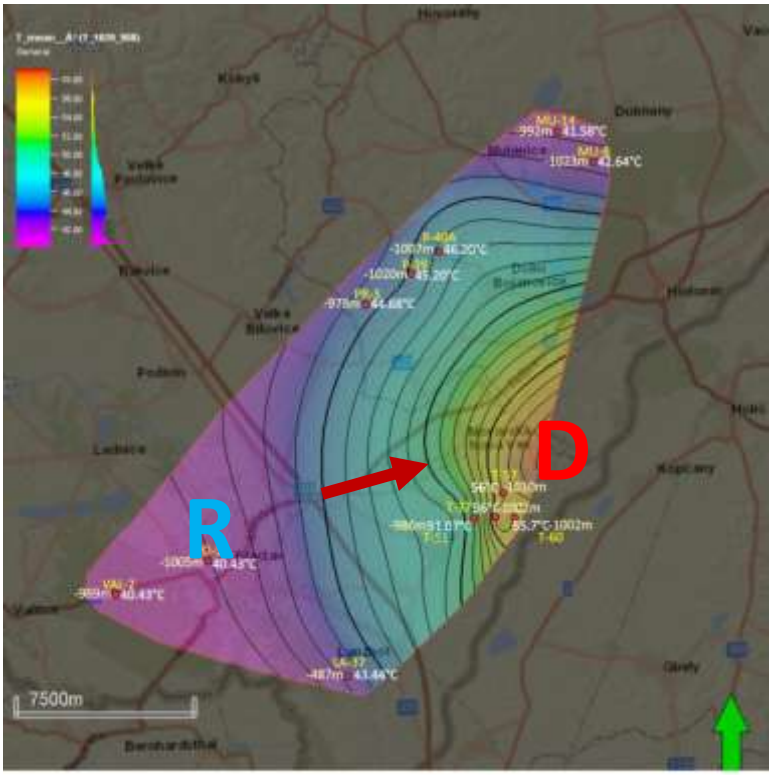

Fig. 12. Temperature distribution at a depth of 1, 000 m in the study area. See Fig. 11 for further explanation.

Temperature contour maps in **Figs. 11-12** are based on data occurring in the region covered by the interpreted reflection seismic profiles 545, 665 and 915. The fluid flow direction interpreted from temperature data is in accordance with such direction interpreted from the stratal geometry imaged by the aforementioned profiles (**Figs. 2-4**).

To further support the interpreted geometry of the topography-driven geothermal fluid flow system, we have also visualized distributions of density and total dissolved solids of encountered fluids. This was done for various specific reservoir horizons from all four studied stratigraphies. This report documents just the outcomes made for horizons populated with the amount of input data that is sufficient for deriving the fluid flow trend.

Therefore, the maps of total dissolved solids in this report are shown for:

1) horizon 26 and basal horizon in the case of the lower Badenian strata;
2) horizon 11 and Láb horizon in the case of the middle Badenian strata;
3) horizons 1-3 in the case of the upper Badenian strata; and
4) horizons 11-14 in the case of the Sarmatian strata.

The documenting maps of density distribution are shown for:

1) horizon 11 and Láb horizon in the case of the middle Badenian strata;
2) horizons 11-14 in the case of the Sarmatian strata.

Maps made for the lower Badenian reservoir horizons indicate that the lower Badenian sediments of the Vienna Basin are represented by several small disconnected volumes of sediment, and, therefore, they cannot host a regional geothermal fluid flow system. In contrast, horizons in middle Badenian, upper Badenian and Sarmatian strata are regionally more-or-less continuous, and they host such a system in the central portion of the basin.

The recharge area interpreted from the decreased values of the total dissolved solids in fluids correlates with recharge area interpreted from temperature data and stratal geometry of the basin fill. The discharge area interpreted from the increased values of the total dissolved solids in fluids correlates with recharge area interpreted from temperature data and stratal geometry of the basin fill. The same is valid for the recharge and discharge areas interpreted from fluid density distribution.

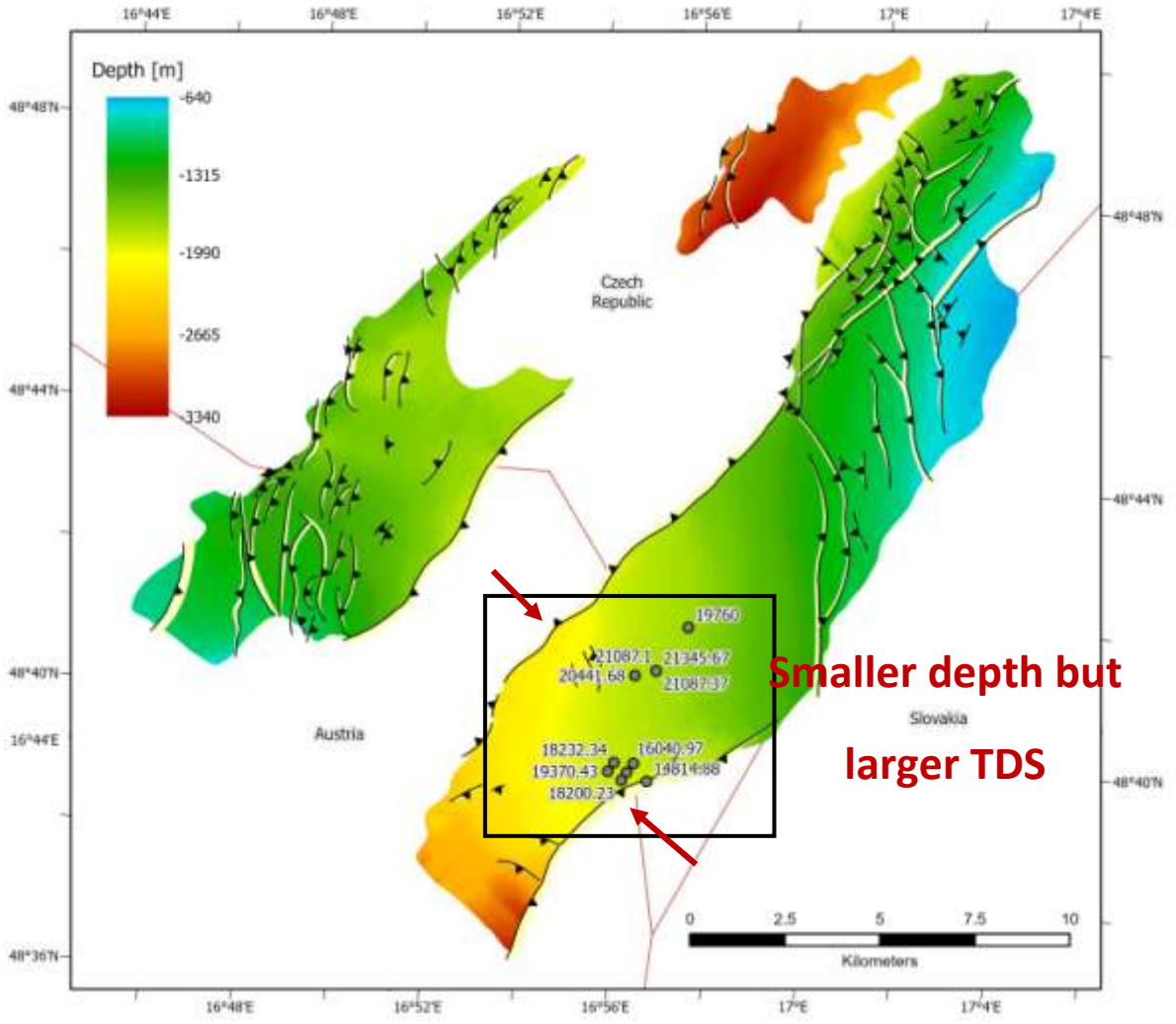

Fig. 13. Point map of the total dissolved solids (TDS in mg/l) in fluids sampled in wells in the lower Badenian horizon 26. Note the implied fluid flow from both sides of the Hodonín-Gbely horst.

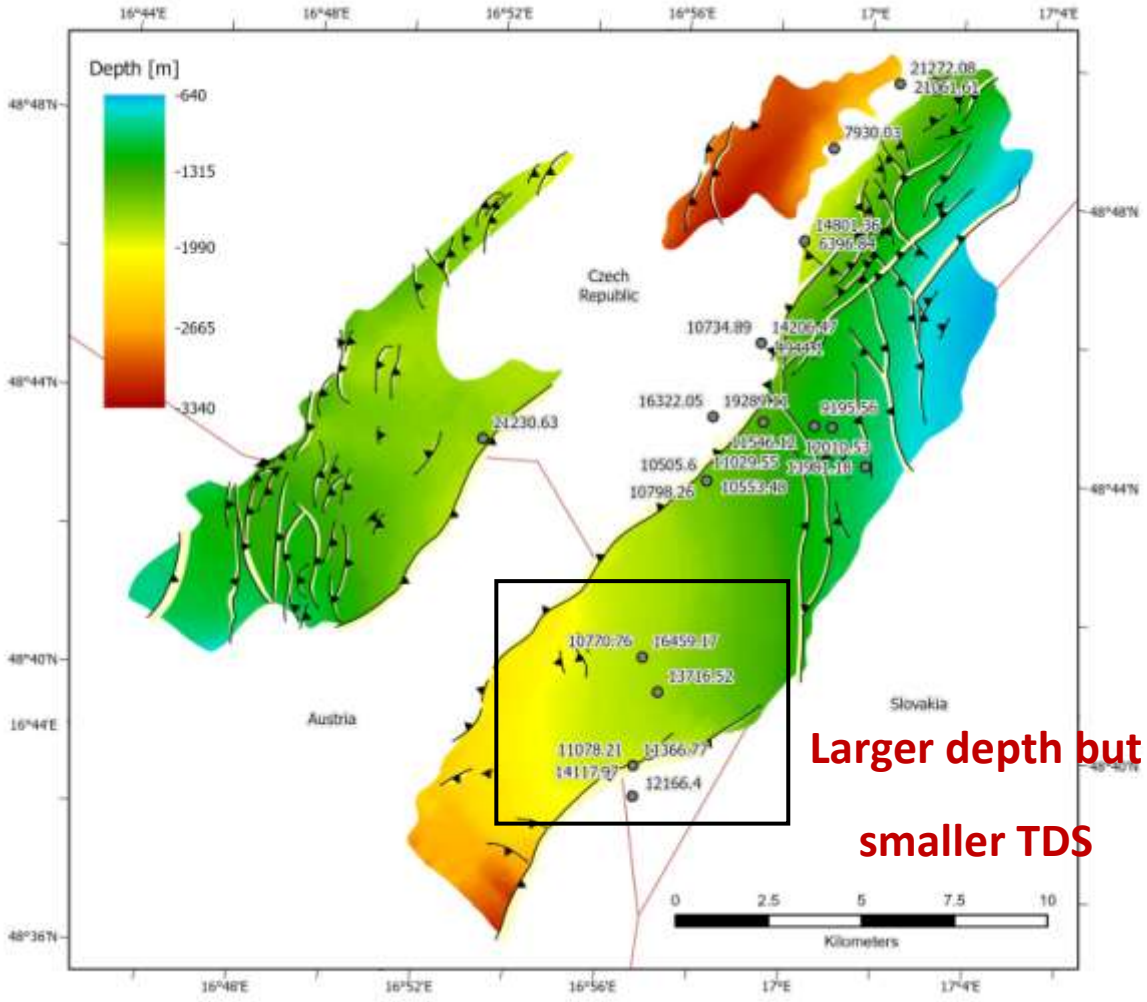

Fig. 14. Point map of the total dissolved solids (TDS in mg/l) in fluids sampled in wells in the basal lower Badenian horizon. Note the colder temperatures than those in horizon 26, despite the fact that the basal horizon is the deeper of the two. In accordance with well data, this map proves that the basin fill is composed of the system of mainly sandy/sandstone aquifers separated from each other by intra-formational shale horizons.

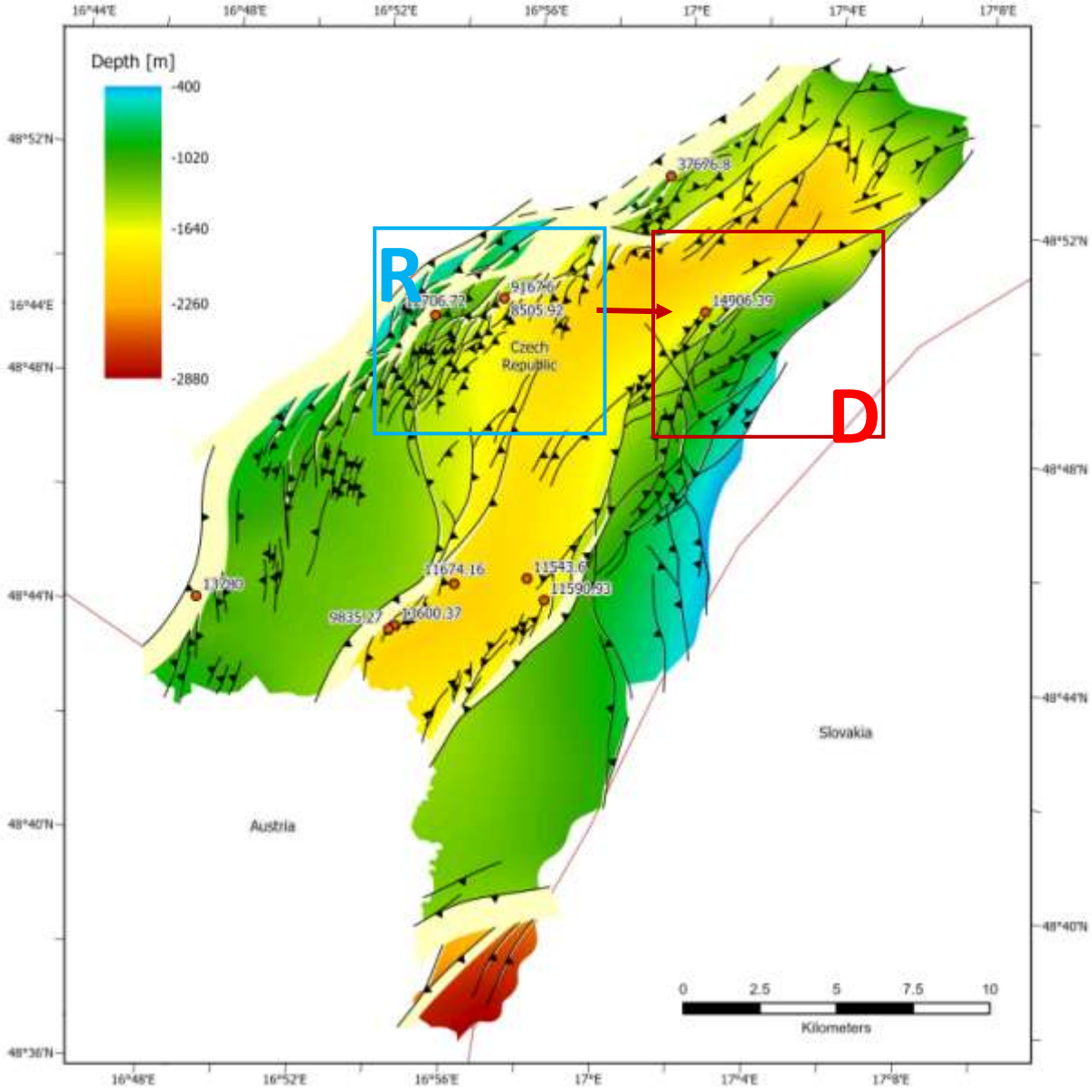

Fig. 15. Point map of the total dissolved solids (TDS in mg/l) in fluids sampled in wells in the middle Badenian horizon 11. Note the decreased values in the recharge area and increased ones in the discharge area.

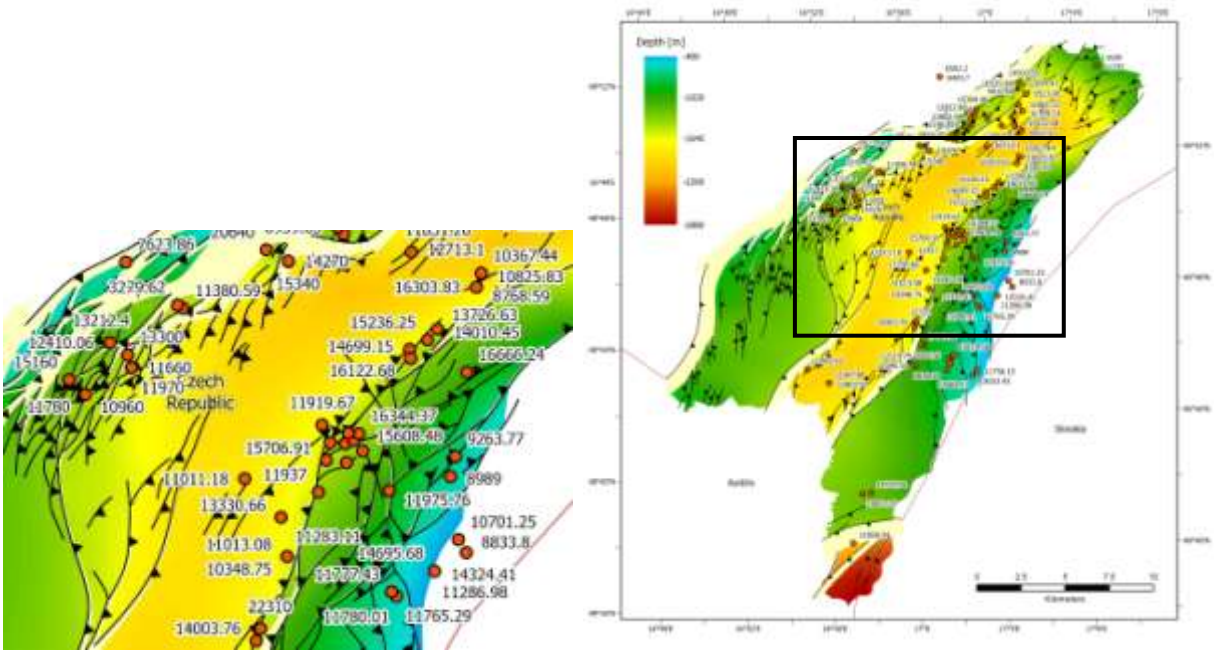

Fig. 16. Point map of the total dissolved solids (TDS in mg/l) in fluids sampled in wells in the middle Badenian Láb horizon. Note the decreased values in the recharge area (3, 279 - 15, 160 mg/l) and increased ones in the discharge area (10, 348 - 22, 310 mg/l).

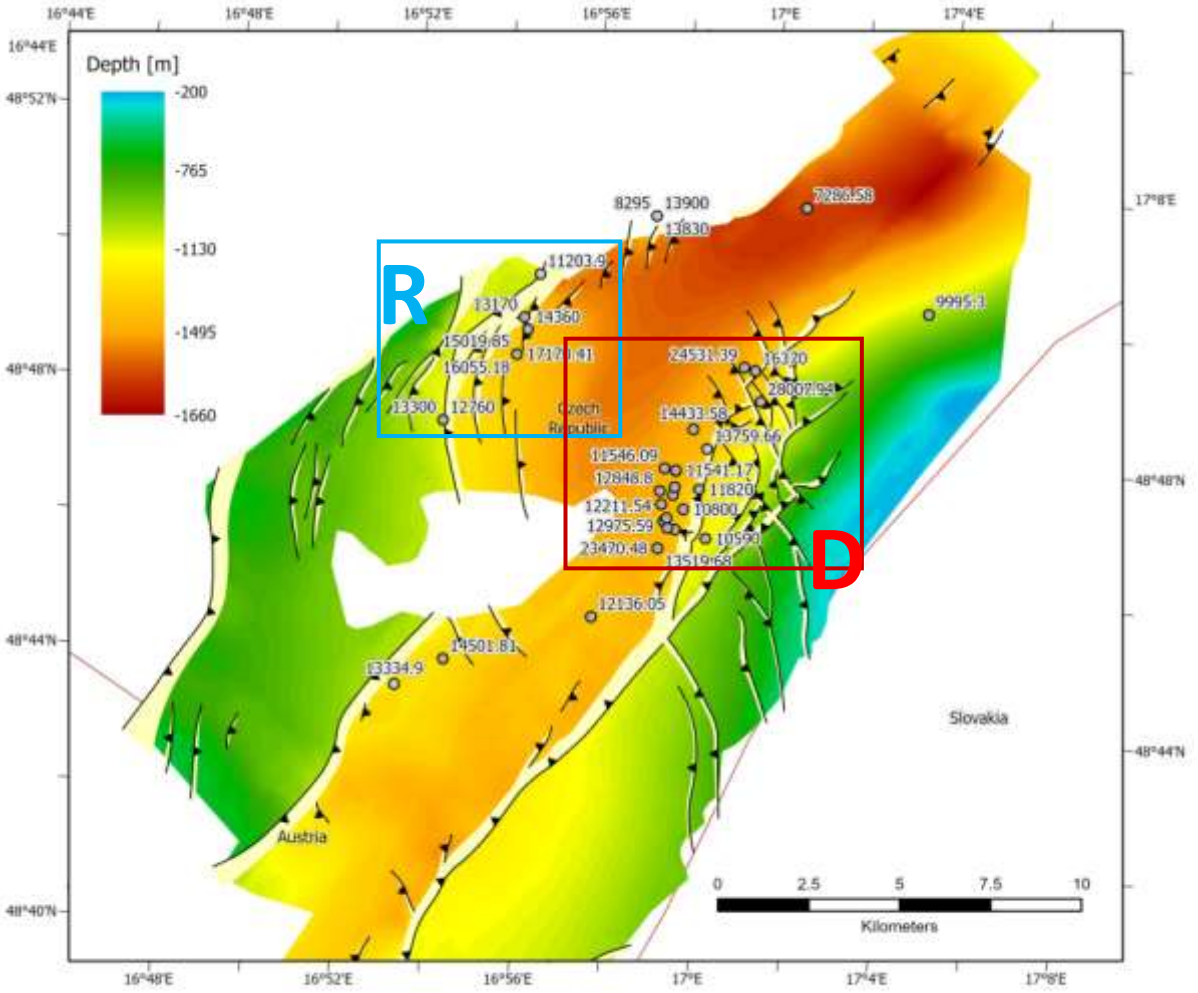

Fig. 17. Point map of the total dissolved solids (TDS in mg/l) in fluids sampled in wells in the upper Badenian horizons 1-3. Note the decreased values in the recharge area and increased ones in the discharge area.

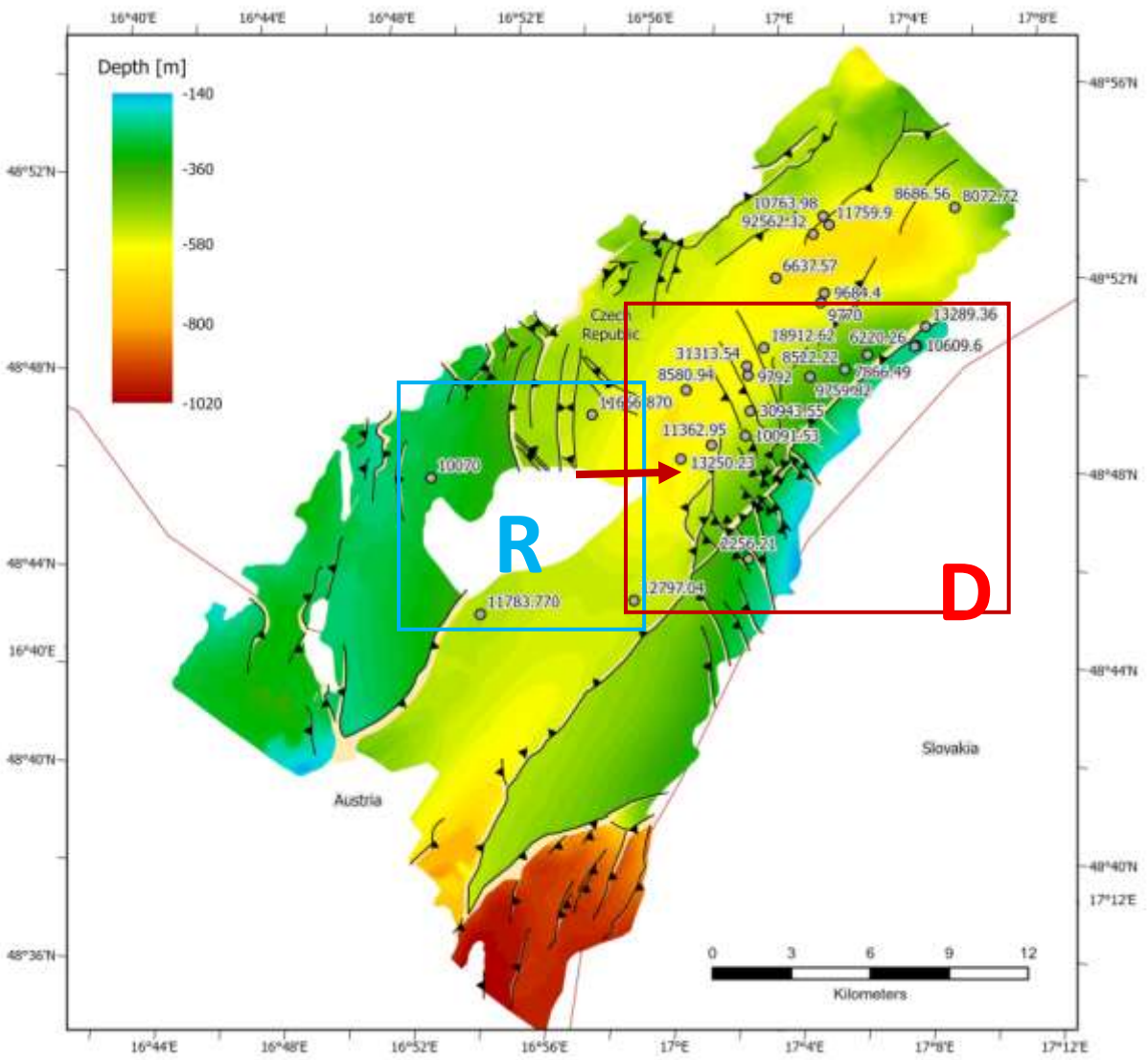

Fig. 18. Point map of the total dissolved solids (TDS in mg/l) in fluids sampled in wells in the Sarmatian horizons 11-14. Note the decreased values in the recharge area and increased ones in the discharge area.

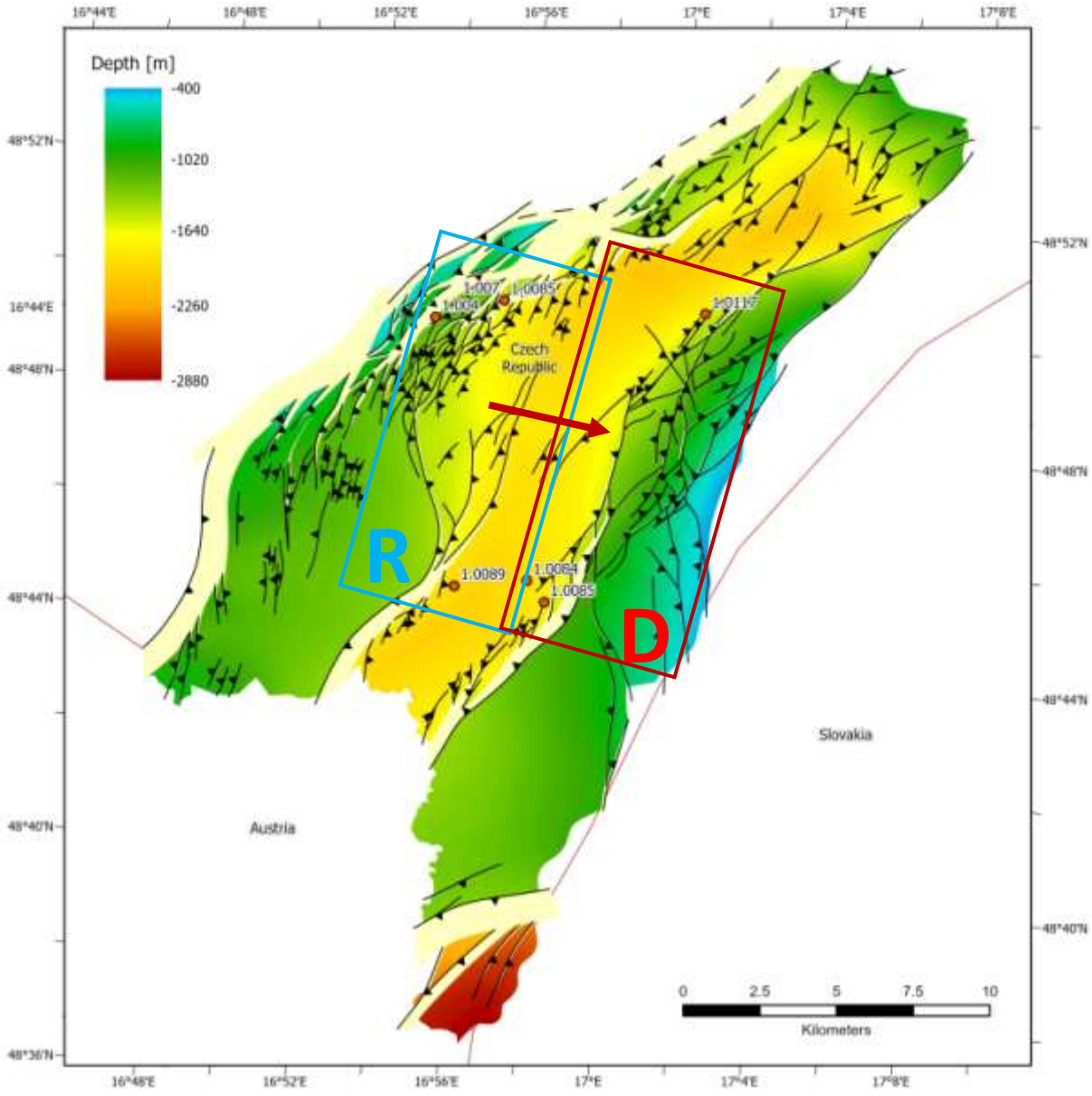

Fig. 19. Point map of the density of fluids (in g/m^3) sampled in wells in the middle Badenian horizon 11. Note the decreased values in the recharge area and increased ones in the discharge area.

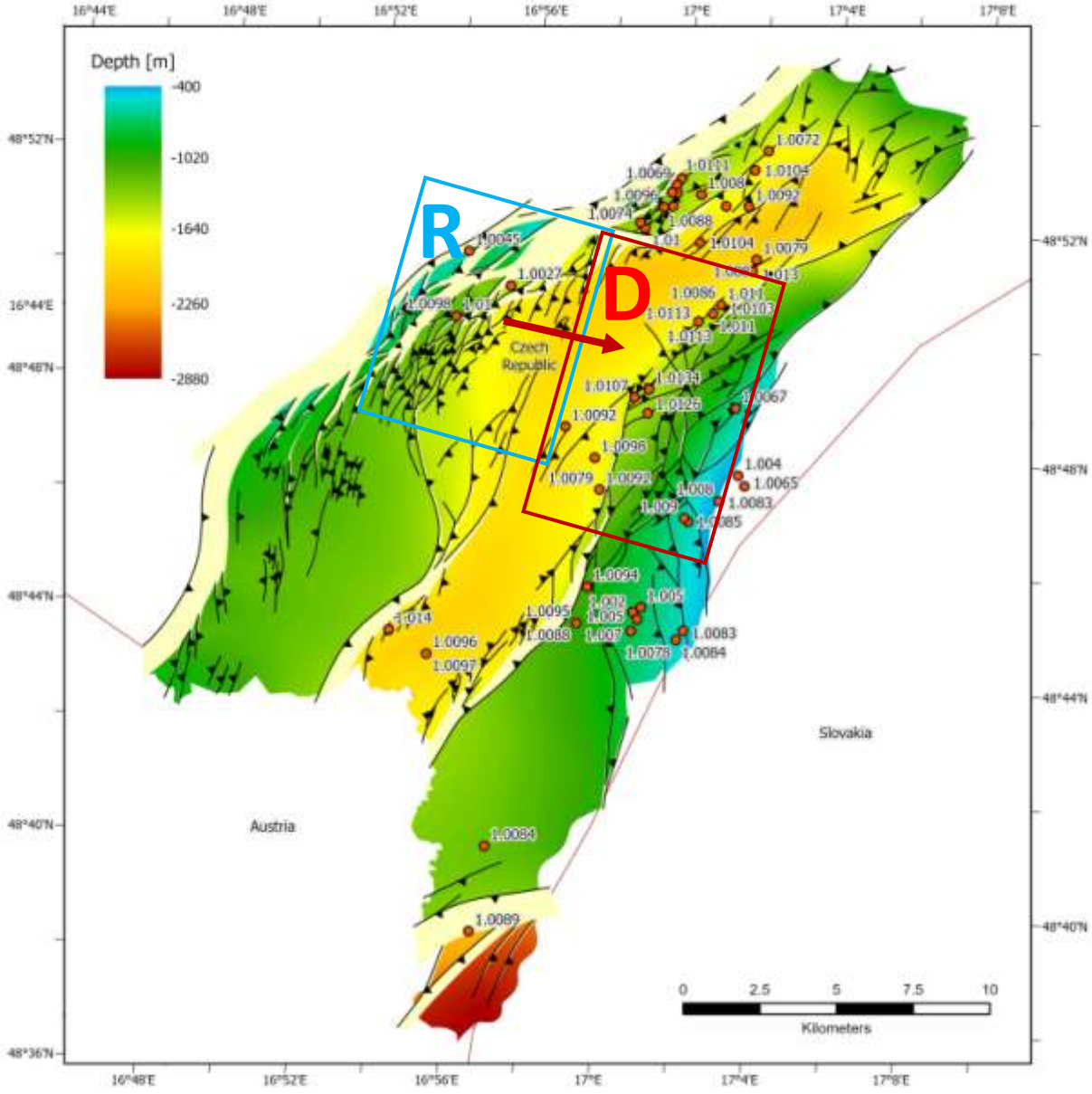

Fig. 20. Point map of the density of fluids (in g/m^3) sampled in wells in the middle Badenian Láb horizon. Note the decreased values in the recharge area and increased ones in the discharge area.

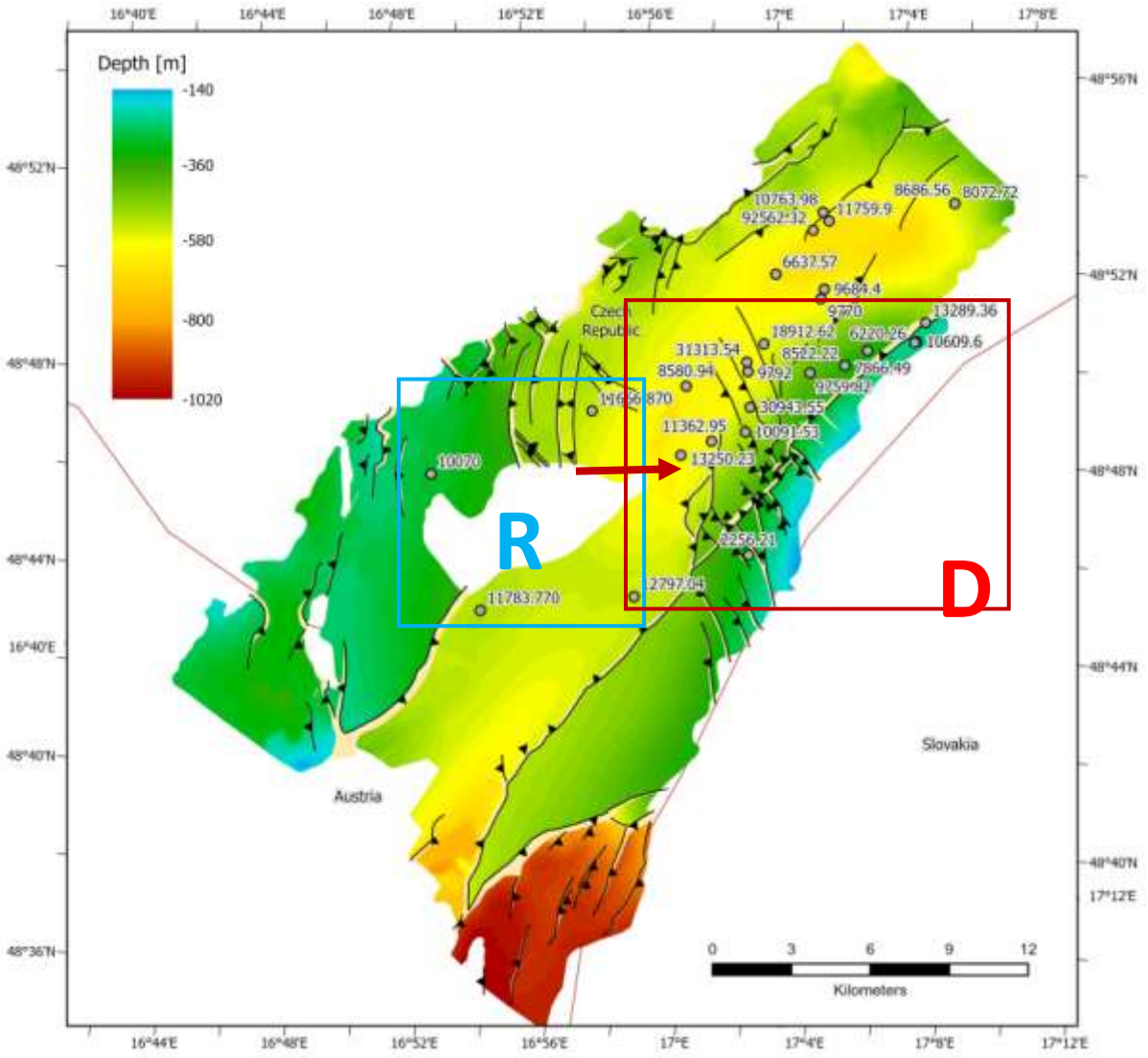

Fig. 21. Point map of the density of fluids (in g/m^3) sampled in wells in the Sarmatian horizons 11-14. Note the decreased values in the recharge area and increased ones in the discharge area.

All data shown above indicate the existence of the topography-driven geothermal fluid flow system, which is located in the central portion of the Czech part of the Vienna Basin (**Fig. 22**). Its recharge area occupies the elevated NW basin flank. Its discharge area includes the marginal faults of the Hodonín-Gbely horst and its summit.

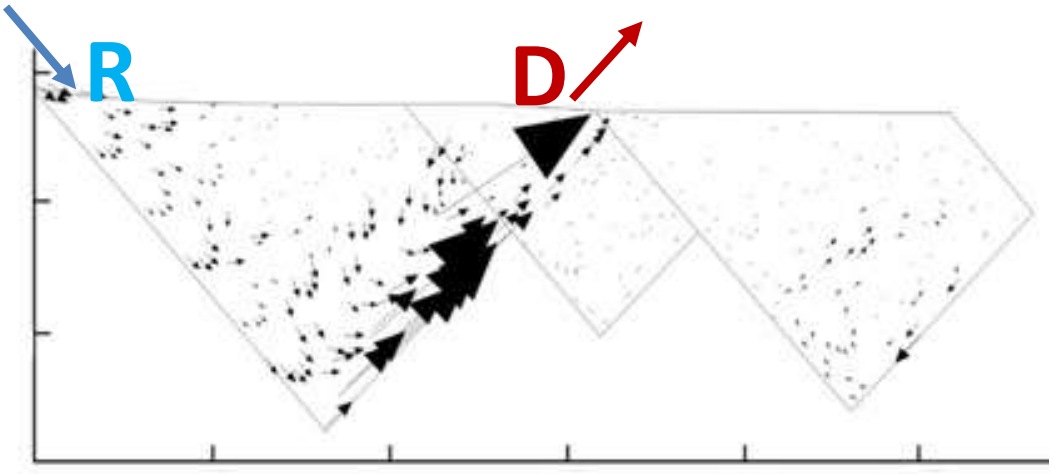

Fig. 22. Schematic figure showing the theoretical topography-driven geothermal fluid flow system, which has the recharge area at basin flank and discharge area at structural high located in the basin center. R – recharge area, D – discharge area.

Parameters and indexes calculated for the development of the play fairway map

The first calculated parameter, which will be used for the construction of the play fairway map of the Czech portion of the Vienna Basin is the Thermoelectric Production Index, represented by the ratio P/P_r (Soldo and Alimonti, 2015). P is the thermal energy of the reservoir, calculated from the equation:

$$P = (\rho_{oil} c_{p\ oil} + WOR * \rho_{water} c_{p\ water})\ Q_t \Delta T/(WOR+1),$$

where ρ is the geothermal fluid density, c_p is the specific heat of the fluid, Q_t is the quantity of the fluid flow, ΔT fluid temperature change, which equals to the temperature of the penetrated reservoir in well minus the average annual surface temperature in the Czech Republic (9.7 ^{o} C in year 2023 according to the web site Statista), and WOR is the water/oil ratio in the geothermal fluid. Pr is the reference value of the energy, which is equal to the output of the ORC power plant. It ranges from 1 to 5 MW according to the power plant type.

The second calculated parameter is the Temperature Flow Rate Index, represented by the ratio q/T (Soldo and Alimonti, 2015). q is the rate of the inflow of the geothermal fluid from the reservoir (**Fig. 23b**) and T is its temperature.

Fig. 23a shows the Arc GIS visualization of the Temperature Flow Rate Index distribution in the case of the middle Badenian Láb reservoir horizon, which is one of the most significant horizons in the study area.

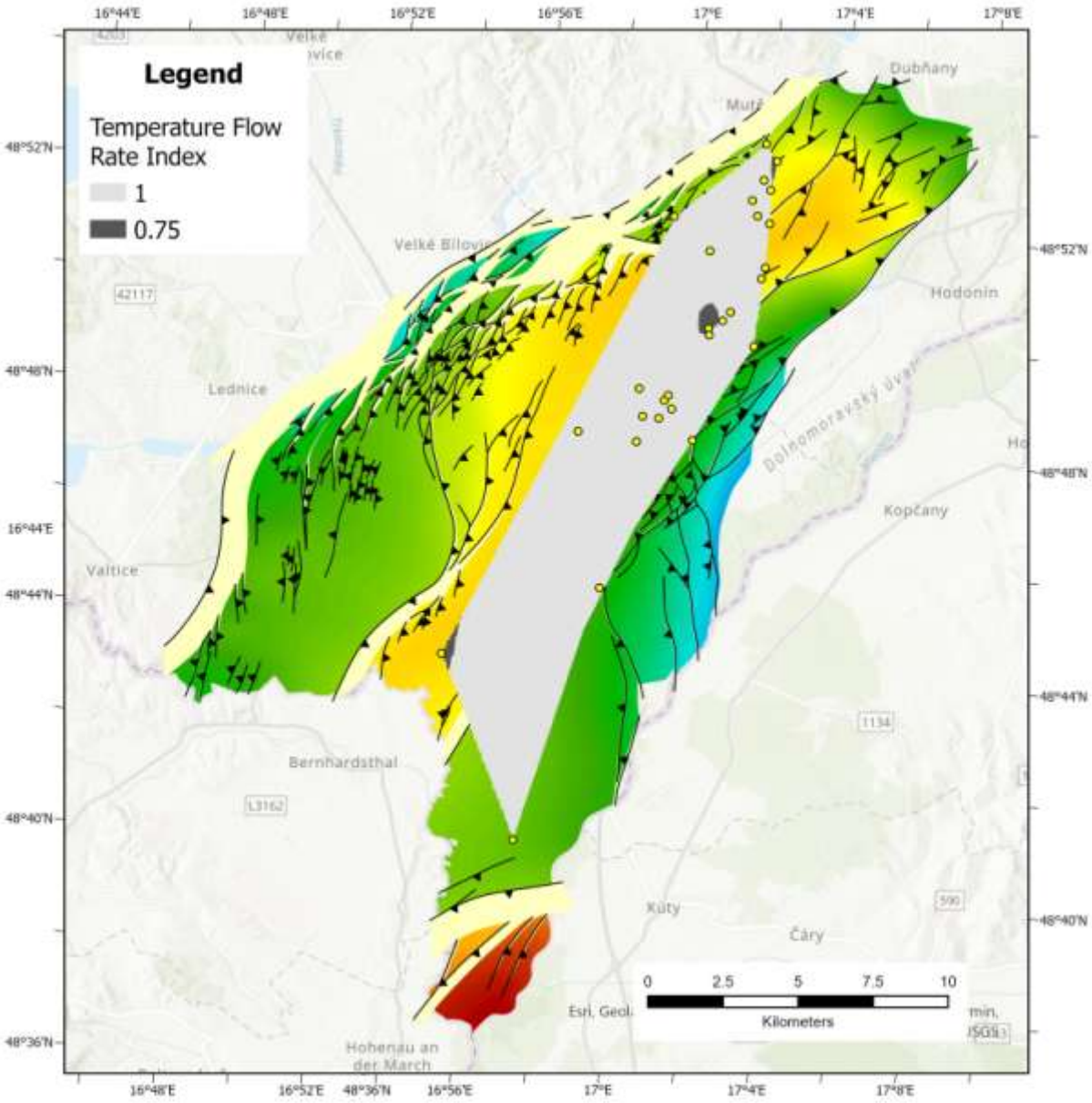

Fig. 23. a) Arc GIS visualization of the Temperature Flow Rate Index distribution from the data on the middle Badenian Láb horizon, which is the most important hydrocarbon reservoir horizon in the Czech portion of the Vienna Basin.

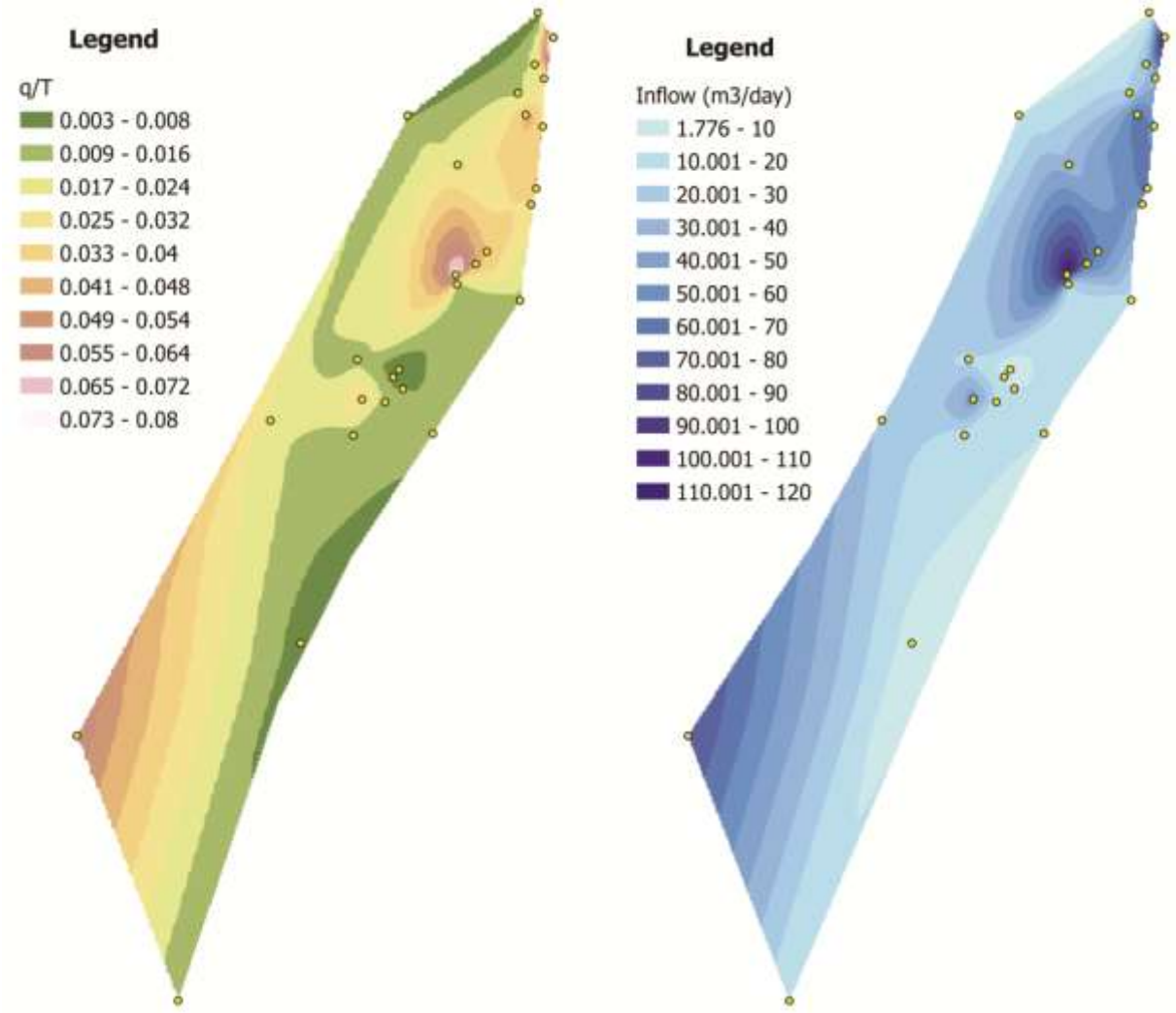

Fig. 23. b) Detail of the visualization of the Temperature Flow Rate Index distribution from Fig. 23a compared to the rate of the inflow of the geothermal fluid from the reservoir. Note the series of distinct inflow rates along the marginal faults of the Hodonín-Gbely horst in the northern part of the contour map.

The third calculated parameter is the Outlet Temperature Index, represented by ratio $T_i/(2T_{min})$ (Soldo and Alimonti, 2015), which correlates the temperature of the geothermal fluid at well outlet with characteristic temperature of the power plant converting the thermal energy of the reservoir into the electric energy.

The fourth calculated parameter is the Pumping Aided Production Index, represented by the ratio E_p/E (Soldo and Alimonti, 2015). E_p is the electric energy consumed by geothermal fluid pumping from well into the power plant. E is the electric energy produced by the power plant. E is calculated from the thermal energy of the reservoir, P, the calculation of which is discussed above, in the text on the First calculated parameter. E is calculated from the equation:

$E = \eta_u * W_A$,

where η_u is the factor controlling the effectiveness of the conversion of the thermal energy provided to the power plant into the electric energy. W_A is the thermal energy. W_A is calculated from the thermal energy of the reservoir, P, where P is multiplied by the recovery factor (recovery of the geothermal fluid from the reservoir). We are using the value of 20%. The calculation is further controlled by the capacity factor, because the geothermal fluid input into the power plant is not 100% annually, but 80%, which is the decrease caused by the production interruption during the maintenance of the production system. Other factors influencing the calculation are the power plant life span, represented by 20 years, and the geothermal fluid temperature decrease with time, represented by the value of 1^{o} C per year.

We did not create the ***Corrosion Factor***, because geothermal fluids in Czech hydrocarbon fields of the Vienna Basin are proven by the long-term production to be noncorrosive. Their corrosive effect is so minimal that their influence on the power plant during its 20 year-long life cycle can be neglected. The same is valid for the ***Formation Damage Factor*** used for the reservoir undergoing the geothermal fluid production.

As indicated by the aforementioned long-term production, the ***Cementation Factor*** also lacks any distinct influence. The effect of the cementation (in rare exceptions from this observation) is usually suppressed by the well furnishing using fiberglass or stainless steel casing. Other alternative is the use of the anticorrosion coating.

The last calculated parameter is the Cost Index, represented by the time needed for the payback of the (1) initial investment into the power plant, (2) investment into the construction of the entire production system, (3) cumulative cost of each year's maintenance and (4) cumulative cost of the energy consumed on the production system activity.